



Flashover Discharge on Solar Arrays: Analysis of Discharge Current and Image

Tepei Okumura,* Mitsuru Imaizumi,† Kumi Nitta,‡ and Masato Takahashi§
Japan Aerospace Exploration Agency (JAXA), Tsukuba 305-8505, Japan

and

Tomonori Suzuki¶ and Kazuhiro Toyoda**
Kyushu Institute of Technology, Kitakyushu 804-8550, Japan

DOI: 10.2514/1.50907

Electrostatic discharge tests were performed on large solar array panels under the simulated plasma environments of a geostationary orbit and a low Earth orbit to investigate the propagation length and velocity of flashover plasma. To investigate the propagation length, the neutralized current on the strings was also examined. The neutralized charge value due to flashover plasma was found to decrease with distance. Propagation length was limited under both the geostationary orbit environment and the low-Earth-orbit environment. Visual investigation of the velocity of flashover plasma clarified that velocity decreases with time. The initial velocity of flashover plasma measured was several tens of km/s, regardless of orbital environment conditions.

Nomenclature

C_{ext}	=	external capacitance, F
I_b	=	blowoff current, A
I_{peak}	=	peak of primary discharge, A
I_{st} to I_{stn}	=	flashover current and neutralized current, A
L_p	=	propagation length, m
T_{arc}	=	primary discharge duration, s
T_{delay}	=	delay time for the gate signal, s
T_{gate}	=	gate time for image intensifier, s
t_{i1}, t_{i2}	=	start and end time of primary discharge current, s
Q_{arc}	=	discharge charge, Q
V_b	=	bias voltage, V
V_p	=	propagation velocity, m/s

I. Introduction

ELECTROSTATIC discharge on a solar array may lead to solar cell junction degradation [1–3] and a secondary arc [4,5]; therefore, electrostatic discharge (ESD) has been studied for years. Figure 1 illustrates the current flow of an ESD on a spacecraft. ESD is triggered by a blowoff discharge attributed to spacecraft capacitance. The blowoff discharge leads to flashover discharge on a solar array. The energy source of flashover discharge is the capacitance of the cover glass and the solar array panel's insulation sheet. Because the spacecraft capacitance (in the order of several hundred picofarads) is not as great as the capacitance of the cover glass and insulation sheet (in the order of microfarads), flashover discharge is the major current

Received 24 May 2010; revision received 17 November 2010; accepted for publication 6 December 2010. Copyright © 2010 by the American Institute of Aeronautics and Astronautics, Inc. All rights reserved. Copies of this paper may be made for personal or internal use, on condition that the copier pay the \$10.00 per-copy fee to the Copyright Clearance Center, Inc., 222 Rosewood Drive, Danvers, MA 01923; include the code 0022-4650/11 and \$10.00 in correspondence with the CCC.

*Postdoctoral Fellow, Institute of Aerospace Technology; okumura.tepei@jaxa.jp.

†Associate Senior Engineer, Institute of Aerospace Technology; imaizumi.mitsuru@jaxa.jp.

‡Associate Senior Engineer, Institute of Aerospace Technology; nitta.kumi@jaxa.jp.

§Senior Engineer, Institute of Aerospace Technology; takahshi.masato@jaxa.jp.

¶Graduate Student, Department of Electrical Engineering; f106076t@tobata.isc.kyutech.ac.jp.

**Associate Professor, Department of Electrical Engineering; toyoda@ele.kyutech.ac.jp.

source of ESD energy. As mentioned, because ESD is a well-known cause of an anomaly on the solar array system [6,7], an ESD test is required before launch to guarantee the quality of the solar array design. In a typical ESD test, a small-scale solar array panel is used. To perform a representative ESD test on a small solar array panel, it is necessary to simulate an accurate flashover current [8,9]. To simulate the current, we need the characteristics of the flashover discharge, such as the velocity of flashover plasma and propagation area. However, these characteristics are not well clarified. Therefore, an ESD test on a large solar array panel is also necessary.

Several authors have published the results of their experiment on flashover discharge [10–13]. All authors showed that the velocity of flashover plasma is in the order of 10^4 m/s. Masui et al. showed that flashover plasma decelerates and proposed a flashover current estimation method. However, from earlier experiments, Amorim and Leung proposed that the velocity of flashover plasma is constant. The problem with their experiments was the size of solar array panel. The maximum area of their solar array panels was 1 m^2 [10–13]. Because flashover discharge is an event in the order of several hundred microseconds, we needed a larger panel to investigate the accurate velocity of flashover plasma.

We prepared two $1.2 \times 2 \text{ m}$ solar array panels. A vacuum chamber was used to simulate both the plasma environments of geostationary orbit (GEO) and low Earth orbit (LEO). In [10–12], a surface potentiometer was used to measure the change under an inverted voltage gradient condition. Although a surface potentiometer is suitable for investigating the propagation area of flashover plasma, the measurement time is not short enough. Especially, in the case of large solar array panels, the measurement time becomes long. Thus, we used a current probe to investigate the propagation area of flashover plasma. To measure the velocity of flashover plasma, we used a camera with an image intensifier (II). Our experiment method is explained in chapter B. In chapter C, the experimental results under the simulated GEO plasma environment are discussed. In chapter D, the experimental results under the simulated LEO plasma environment are discussed. In chapter E, we summarize our experimental results.

II. Experiment

A. Solar Array Coupon

Figure 2 depicts the solar array panel for this experiment. The size is 2 m in length and 1.2 m in width; the area is 2.4 m^2 . The design of the solar array panel is flight qualified. The edge of solar cell is glued by silicon adhesive; the interconnectors are exposed to space. Although the thermal cycle test was performed earlier we cannot see

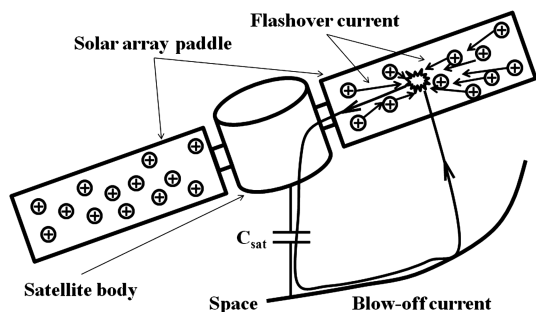


Fig. 1 Blowoff current and flashover current.

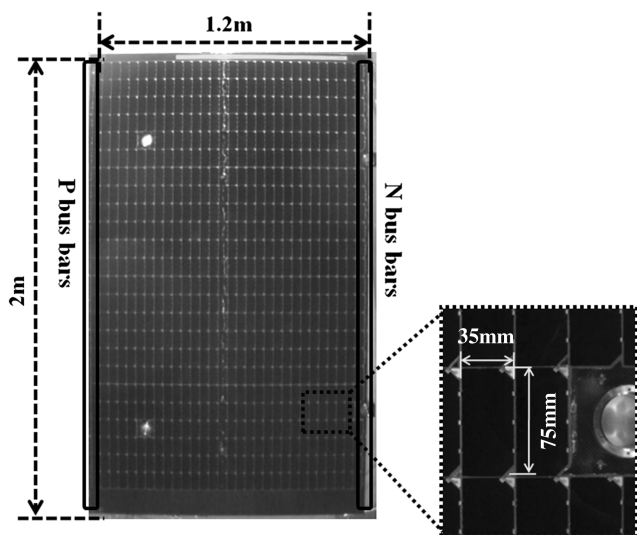


Fig. 2 Solar array panel.

any degradation on the adhesive or cover glass on the solar array panel. Seven hundred InGaP/GaAs/Ge triple-junction solar cells (3J cells) are attached to each solar array panel. There are 24 strings on each panel, that is, 29 or 30 solar cells are connected in series in each string. The total number of solar cells on a solar array panel is 715. The bus bars on each string are insulated by polyimide tape. Every solar cell has a 100- μm -thick cover glass with antireflection (AR) coating on its surface. The size of each solar cell is approximately 35×70 mm and 27.56 cm² in area. Figure 3 shows the solar array coupons inside the vacuum chamber. The object between the solar array panels and the chamber wall is polyimide film (25 mm thick), which insulates the substrate of the solar array panel from the chamber wall. We used two solar array panels with a gap of 0.06 m between the two panels; the total area for the experiment is

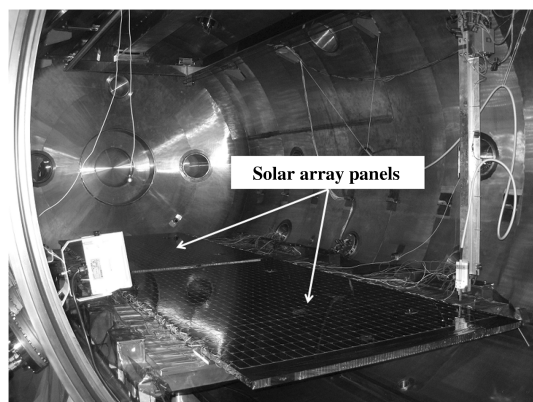


Fig. 3 Solar array panels in vacuum chamber.

approximately 4.8 m². The gap length between the panels simulates the gap between the panels of spacecraft.

B. Experimental Environment

The size of the vacuum chamber is 2.5 m in diameter and 4 m in length. The chamber is equipped with two cryogenic vacuum pumps, two electron beam (EB) guns, and an electron cyclotron resonance (ECR) plasma source.

In the high-energy EB experiment representing the GEO environment, the pressure ranged from 5×10^{-5} to 1×10^{-4} Pa. A thin-film aluminum foil (100 nm) was set in front of the EB guns to scatter the electrons. The current density distribution on the solar array coupon ranged from 1 to 50 $\mu\text{A}/\text{m}^2$. We irradiated the solar array panels continuously with the EB during the test. The acceleration voltage was set at 9 kV. Electrons lose approximately 2 keV when they penetrate the aluminum foil and the solar array coupon was biased to -6 kV. Thus, the electron energy was approximately 1 keV when the electrons reached the surface of the solar array panels. The electron loses 2 keV to penetrate the Al foil in our experience. The secondary electron emission coefficient peaks at 1 keV. Consequently, the inverted voltage gradient was generated in the cover glass.

In the plasma environment representing LEO, the pressure was approximately 9×10^{-5} Pa during the experiment. The ECR plasma source generated Xe plasma with a density of 4×10^{11} and 9×10^{10} m⁻³ at 1 and 3.5-m distances from the ECR plasma source; the electron temperature was from 0.8 to 2 eV. The bias voltages were -200 , -500 , -800 , and -1000 V. We started the test at $V_b = -200$ V, and then increased the V_b to -1000 V.

C. Measurement System and Discharge Circuit

Figure 4 illustrates the measurement system and the discharge circuit. A 32-channel oscilloscope was used to measure the voltage and current waveforms. We used current probes to measure the discharge current. The oscilloscope outputs the signals when discharges occur. The output signals are sent to the image capture system with an infrared radiation (IR) camera. Therefore, we can identify the discharge position immediately after a discharge.

To investigate the velocity of flashover plasma propagation, we used the IR camera with an II as Masui et al. did [11]. Kawasaki et al. indicated that cover glass with AR coating emits photon illumination when electrons of flashover plasma hit the cover glass surface [10]. Figure 5 illustrates the measurement system of the IR camera with II and the signal timing chart. The image is captured by the IR camera when the system receives the signal from the oscilloscope. We input a gate signal to activate the IR camera with time delay, T_{delay} . The exposure time is T_{gate} . In our experiment, T_{gate} was set for 1 μs . We generated the gate signal using a delay pulse generator. The oscilloscope was triggered after several microseconds of discharge inception. Therefore, T_{delay} was not exactly relative to discharge inception. The trigger source of the 32-channel oscilloscope was a voltage probe to measure the bias voltage. To minimize the time difference between discharge inception and trigger, we set the trigger level at -5.5 kV.

A high-voltage power supply, V_b , represents the spacecraft potential against ambient plasma. External capacitance, C_{ext} , usually represents spacecraft capacitance. For a commercial satellite of typical size, the C_{ext} is calculated in the order of several hundred picofarads. In this experiment, C_{ext} was 240 pF, but the value does not represent any particular spacecraft. In Fig. 6, the discharge circuit is indicated in detail. We used a high-voltage probe to measure voltage waveforms. A blowoff current was measured by current probe I_b . As mentioned, we have 48 strings. Twenty-six current probes, $I_{\text{st}1}$ to $I_{\text{st}26}$, independently measure the current on each string. Therefore, $I_{\text{st}1}$ to $I_{\text{st}26}$ can measure the actual flashover current and neutralization current. Because we cannot measure the current independently on the other 22 strings, the 22 strings are coupled and the current is measured at I_{uni} .

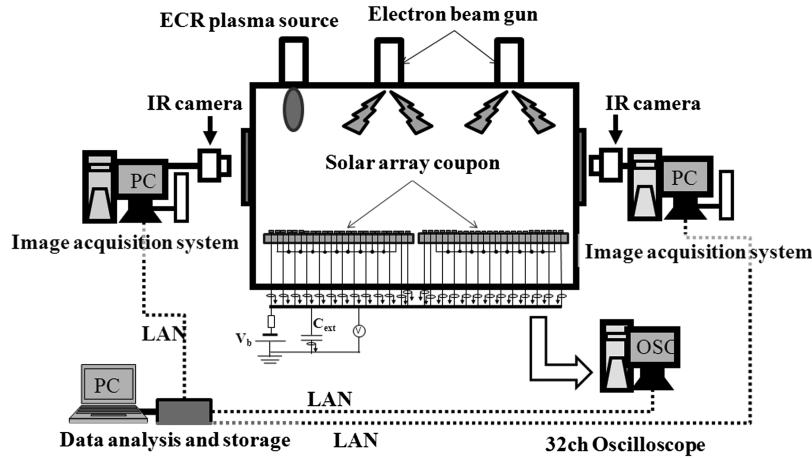


Fig. 4 Measurement system.

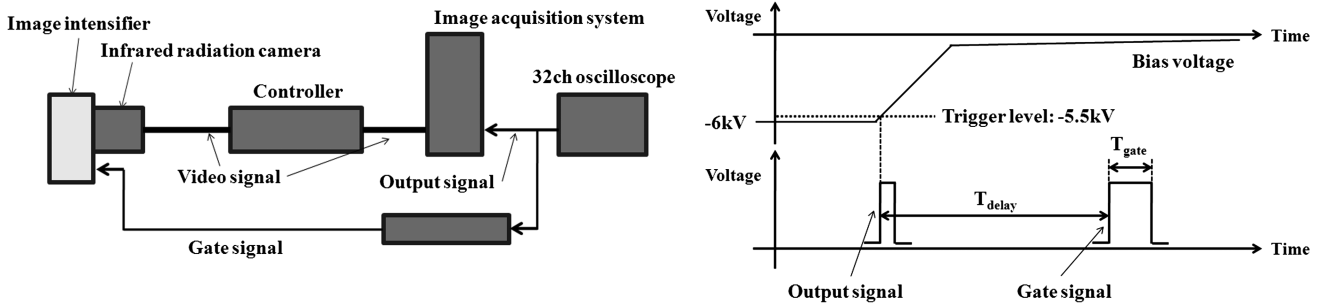


Fig. 5 IR camera with II image acquisition system and timing chart.

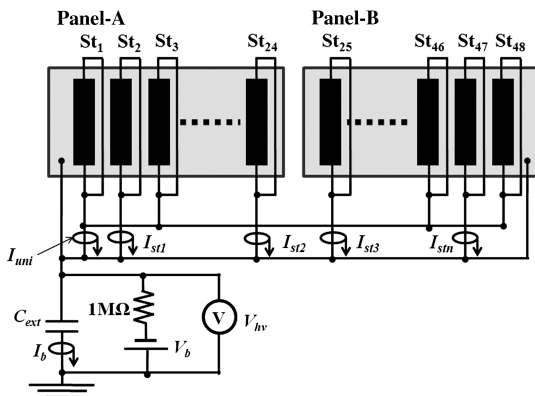


Fig. 6 Discharge circuit.

III. Propagation Length of Flashover Plasma

A. Flashover Current and Definition of Propagation Length

Figure 7 illustrates an equivalent circuit of the solar array. In Fig. 7, the capacitance represents the capacitance of the cover glass. In the equivalent circuit of the solar array, the diode represents the solar cell. However, solar cells on the equivalent circuit are not presented because the solar cells do not contribute to the flashover discharge. As described in the introduction, we used the neutralized current to investigate the propagation length. Once a blowoff discharge occurs on a solar array, the flashover discharge propagates on the surface of the solar array. As a result, the cover glasses supply charge to the discharge spot. As we measure the currents of the strings using the current probes, we can estimate the propagation length from the neutralized charge on the strings.

Figure 8 shows flashover, neutralized, and blowoff currents under the GEO environment. Here, we define the discharge parameter. The

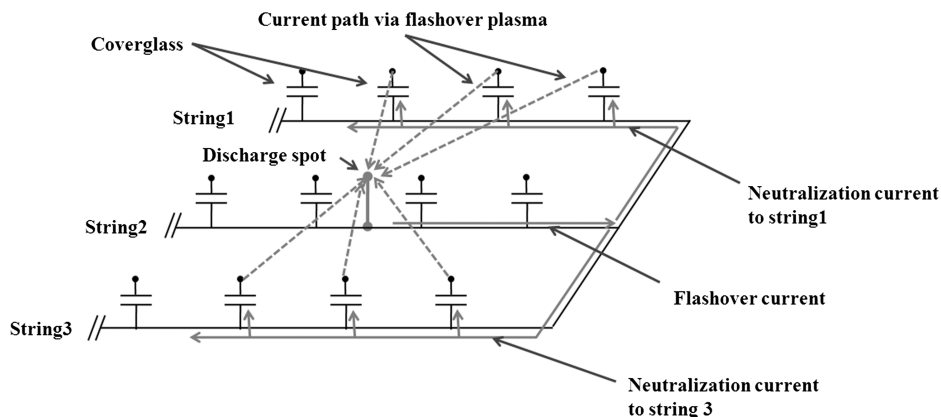


Fig. 7 Equivalent circuit of solar array with current path of neutralized current and flashover current.

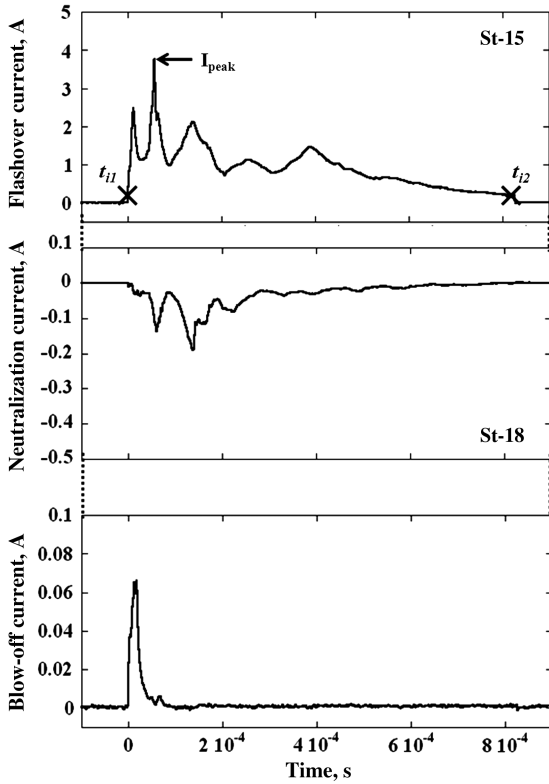


Fig. 8 Flashover current, neutralized current, and blowoff current under the GEO environment.

peak of the current is I_{peak} . We defined t_{i1} and t_{i2} as the time when the current is 5% of I_{peak} . The duration of a discharge, T_{arc} is

$$T_{arc} = t_{i2} - t_{i1} \quad (1)$$

The charge of a discharge, Q_{arc} is

$$Q_{arc} = \int_{t_{i1}}^{t_{i2}} I(t) dt \quad (2)$$

We identified a current waveform that has more than 7×10^{-7} C of charge as the neutralized current. Therefore, the propagation length is defined as the length between the discharge spot and the string where we observed the minimum neutralized current.

Figure 9 shows a typical flashover current waveform under the LEO environment. The flashover current rapidly increases after discharge initiation, and then decreases. The flashover current waveform under the GEO environment was similar to that under the LEO environment. The relationship between the neutralized charge and the distance from the discharge spot under the GEO and LEO environments is shown in Figs. 10 and 11. The graphs in Figs. 10 and

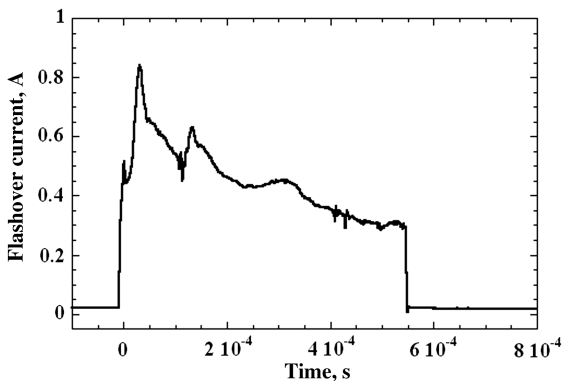


Fig. 9 Typical flashover current waveform under the LEO environment.

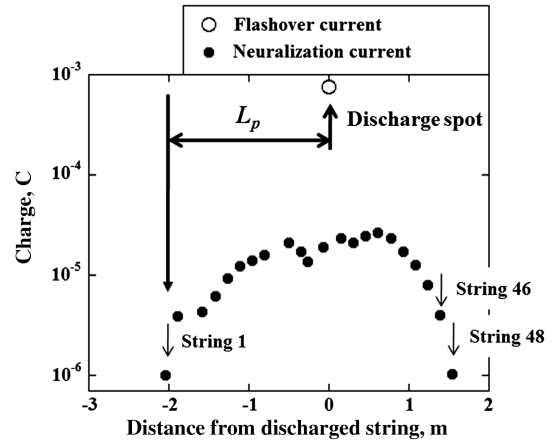


Fig. 10 Relationship between the charge of neutralized current and discharge spot under the GEO environment.

11 show neutralized charge distribution. As can be seen, the neutralized charge decreases with an increase in distance in both environments. In Fig. 10, the neutralized charge disappears before St-48. In Fig. 11, the neutralized charge disappears between St-38 and St-48; the current at St-37 was not independently measured. This fact suggests that the flashover plasma does not reach the edge of the solar array panel. The neutralized charge distribution and flashover current are shown in Figs. 12 and 13 to investigate the effect of discharge position in the GEO and LEO environments. We discuss the data in LEO environment with $V_b = -800$ V in detail in this paper. The marks on the solar array indicate the discharge spot that we identified from captured images. The discharges in the GEO environment were named D01 to D06, and those in the LEO environment D07 to D12. Each discharge is shown with the beam irradiation time from last discharge. It should be noted that the origin of length of neutralized charge distribution always corresponds to string-01. In Fig. 12, the flashover current rapidly increases after discharge inception, and then gradually decreases in any discharge position. In terms of neutralized charge distribution, the neutralized charge decreases with an increase in distance, as shown in Fig. 10. Especially, in the cases of D01 and D06, although the flashover plasma potentially neutralizes for 3.75 m, the flashover plasmas neutralized for approximately 2 m. The beam current density distribution is not uniform on the solar array panel; the current density at the edge of the solar array panel is lower than that at the center. This fact implies that the surface potential distribution on the solar array panel is also not uniform. In the cases of D01 and D06, the neutralized charges near St-01 and St-46 exceed 10^{-5} C. In the cases of D03 and D04, the neutralized charges near St-24 and St-25

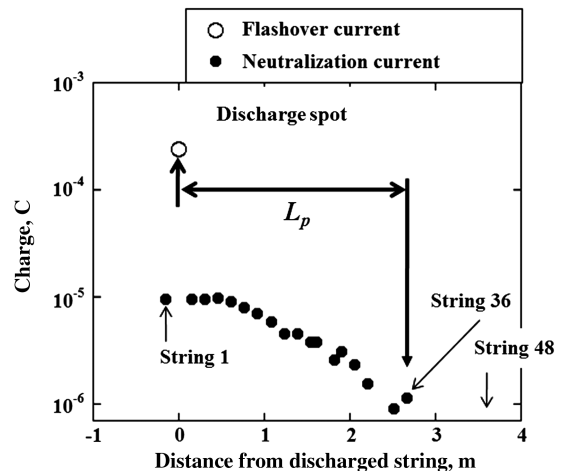


Fig. 11 Relationship between neutralized current and distance from discharge spot under the LEO environment.

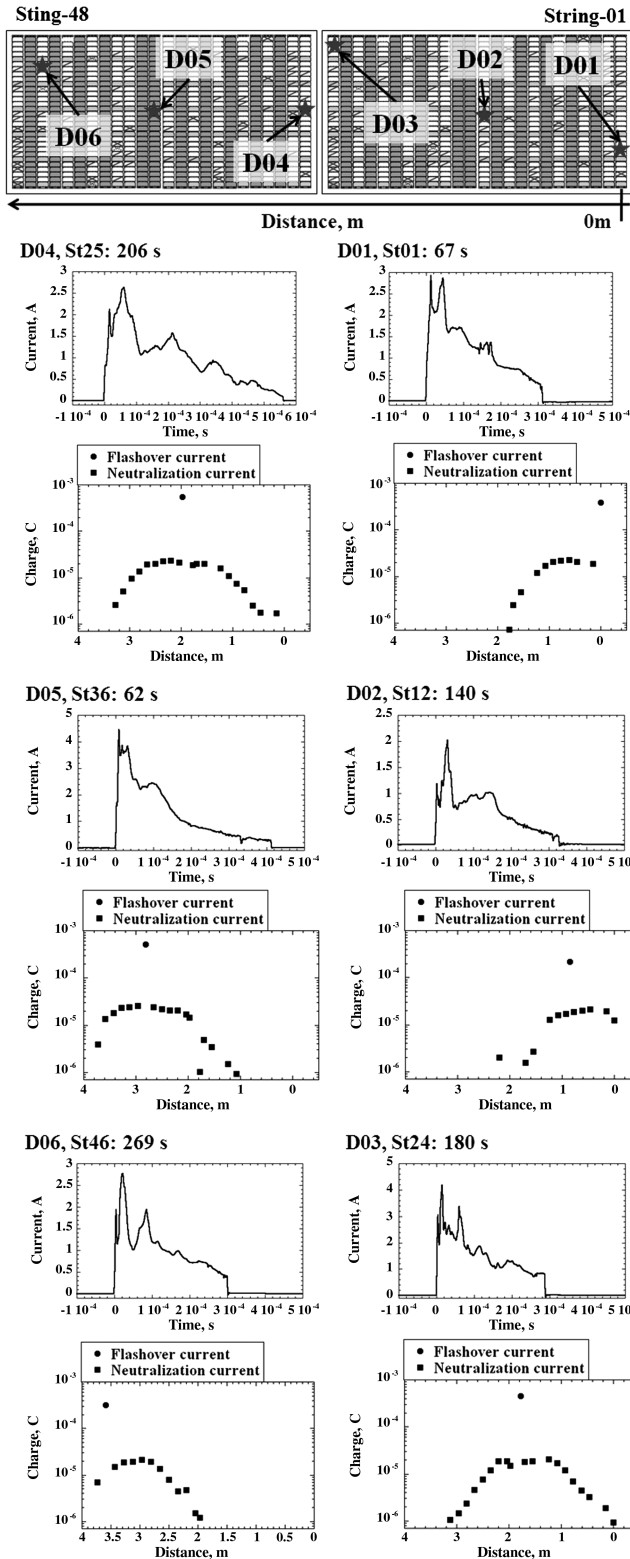


Fig. 12 Flashover current and distribution of neutralized charge in GEO environment.

exceed 10^{-5} C. Because the neutralized charge near the discharged string exceeds 10^{-5} C in any case, uniformity of surface potential distribution is negligible. Because the 2 m from the position of D01 and D06 corresponds to the gap between the solar panels, it is possible to doubt the effect of the gap on neutralized charge distribution. However, when we look at discharges D02 to D05, the flashover plasma neutralizes the strings beyond the gap. Therefore, it is possible to say that the flashover current and neutralized charge distribution do not depend on the position of discharge. In the LEO

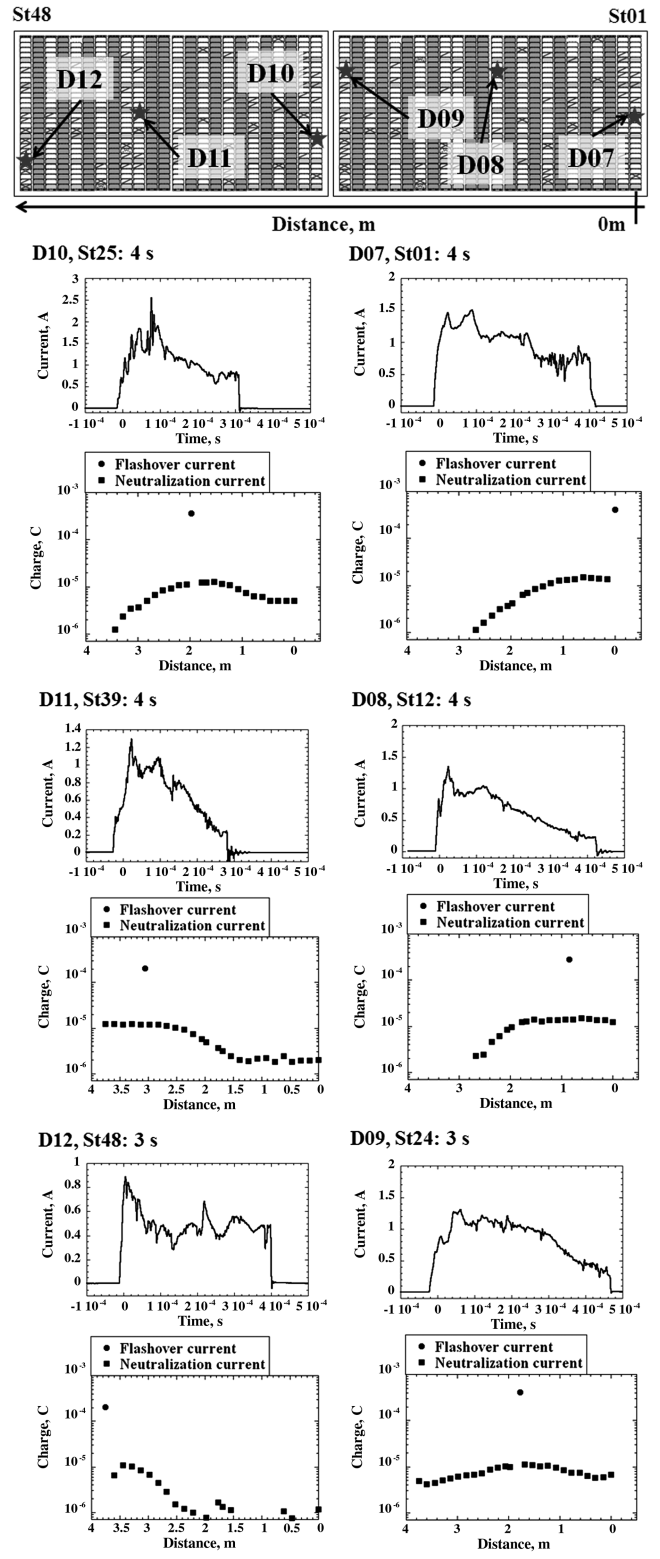


Fig. 13 Flashover current and distribution of neutralized charge in LEO environment.

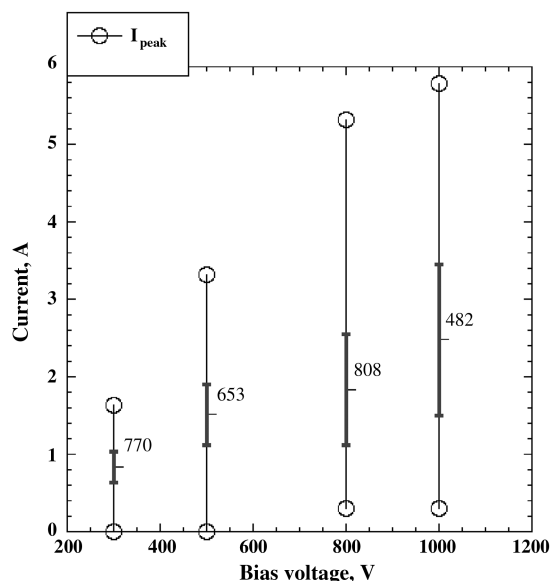
environment, the neutralized charge also decreases with distance from the discharge position. In the cases of D07, D08, and D12, the flashover plasma does not reach the edge of solar array panel. Contrary to these discharges, in the cases of D09 to D11, although the neutralized charge decreases with distance from the discharge position, the neutralized charge does not drop below the threshold value of neutralized charge: 7×10^{-7} C. This fact suggests that the flashover plasma in the LEO environment possibly propagates beyond 3.75 m. In the LEO environment, the plasma density is not

Table 1 Difference of experiment environment

Experiment	Gas	Electron temperature	Plasma density	Pressure
Previous experiment	Argon	X	Order of 10^{10} m^{-3}	$2 \times 10^{-3} \text{ Pa}$
This experiment	Xenon	0.8 to 2 eV	4×10^{11} to $9 \times 10^{10} \text{ m}^{-3}$	$8.8 \times 10^{-5} \text{ Pa}$

uniform as was mentioned. In higher bias voltage, the sheath of an interconnector potentially reaches the chamber wall. Therefore, the effect of the sheath on flashover plasma should be given consideration. The neutralized charge distributions shown in Fig. 13 show us that the neutralized charge near the discharged string exceeds 10^{-5} C at all strings: 800 pF (cover glass capacitance) $\times 30/29$ solar cells $\times 800 \text{ V} = 2 \times 10^{-5} \text{ C}$. This fact suggests that the plasma uniformly charges the solar array panels in higher bias voltage.

Mashidori et al. reported that the L_p of flashover plasma is not limited and neutralizes the entire solar panel surface [14]. A comparison of the experimental conditions between their experiment and ours is shown in Table 1. They used the same facility and solar array panels in their experiment as we did in ours. The main difference was pressure. The pressure of our experiment was significantly lower than that of theirs. This indicated that pressure affects flashover phenomenon. To perform a more realistic experiment to investigate flashover discharges, we must consider pressure. This fact does not suggest that we need to consider pressure in the ESD test to investigate secondary arc or solar cell degradation, because we need to control the current waveform for these tests [8]. Here, the difference of plasma specie may be considered the factor in changing the characteristics of flashover plasma. In fact, the mobility of an Ar ion is greater than that of a Xe ion. However, the mobility of the electron from the discharge spot is much greater than that of those ions. We think the characteristics of flashover plasma do not change with ion specie, because the propagation of the electron from the discharge spot dominates the flashover discharge. We investigated the characteristics of flashover discharge when the bias voltages were -200 , -300 , -500 , -800 , and -1000 V . We show the relationship between bias voltage and peak current (I_{peak}) in Fig. 14. In Fig. 14, the thin error bars represent the maximum and minimum of I_{peak} . The thick error bars represent the standard deviation of average of I_{peak} . The figures in Fig. 14 are the number of discharges for each bias voltage. As can be seen, I_{peak} increases with an increase of bias

**Fig. 14** Relationship between bias voltage and peak current I_{peak} under the LEO environment.

voltage. When the bias voltage is higher, the charge stored on the cover glass is obviously greater, because the bias voltage corresponds to the differential voltage in the cover glass in the LEO environment. Therefore, this result is reasonable. When the solar array generates the current, the potential at the negative end of the solar array against ambient plasma is almost equal to the bus voltage of the solar array in the LEO environment [15]. Therefore, the bias voltage in the discharge circuit is synonymous to the bus voltage in the experiment under the LEO environment. A past ground test reported that the threshold voltage of discharge in LEO was -150 V at bus bar [16]. In Fig. 14, when the bias voltage is -300 V , the average, minimum, and maximum of I_{peak} are 0.84, 0.002, and 1.6 A, respectively. In both environments, we need several microfarads to simulate the flashover current. Assuming the flashover discharge fully neutralizes within a 2-m radius, the value of capacitance is $2 \mu\text{F}$. In Fig. 14, the peak of flashover current does not exceed 6 A, even in the case of -100 V in the LEO environment. In the GEO environment, the flashover current does not exceed 6 A, as shown in Fig. 14. Therefore, we need to control the peak current at its proper value even though we use a large capacitance. Several control methods are described in [8,9].

B. Statistical Analysis of Propagation Length

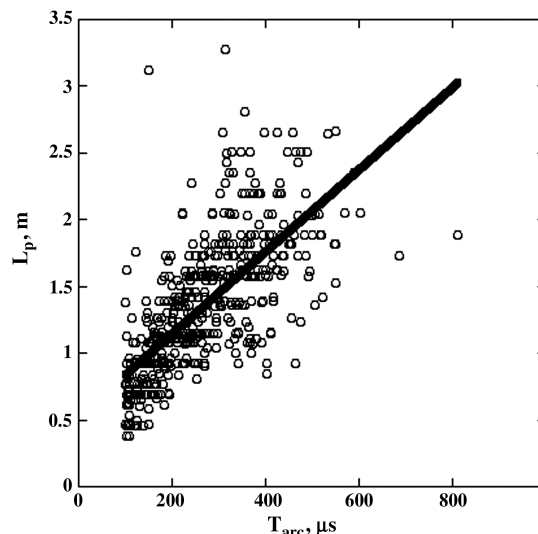
Figure 15 shows the relationship between the T_{arc} and L_p in the GEO environment. The line in the figure expresses the linear regression of L_p , which is expressed as Eq. (3) with the correlation coefficient, R :

$$L_p = 0.54 + 3073.2 \times T_{\text{arc}}; \quad R = 0.70 \quad (3)$$

R ranges from 0 to 1; $R = 1$ is the strongest correlation. Although the greatest L_p was 3.2 m at a T_{arc} of $316 \mu\text{s}$, the line shows that L_p increases with an increase of T_{arc} . In addition, when the T_{arc} was $811 \mu\text{s}$, the L_p was 1.87 m. This suggests that the T_{arc} is not determined by only L_p . There may be other parameters to determine L_p . The distribution of differential voltage on solar panels could be another parameter. However, we did not measure the potential distribution before and after each discharge. Therefore, we could not find another parameter from the experiment.

As discussed, the L_p potentially exceeds 3.75 m in the LEO environment. The discharges between St-01 and St-09 are selected for statistical analysis. Figure 16 shows the relationship between the pulse duration, T_{arc} , and the L_p in the LEO environment with $V_b = -800 \text{ V}$. The line also shows the linear regression of L_p :

$$L_p = 1.18 + 1853.8 \times T_{\text{arc}}; \quad R = 0.53 \quad (4)$$

**Fig. 15** Relationship between pulse duration T_{arc} and L_p under the GEO environment.

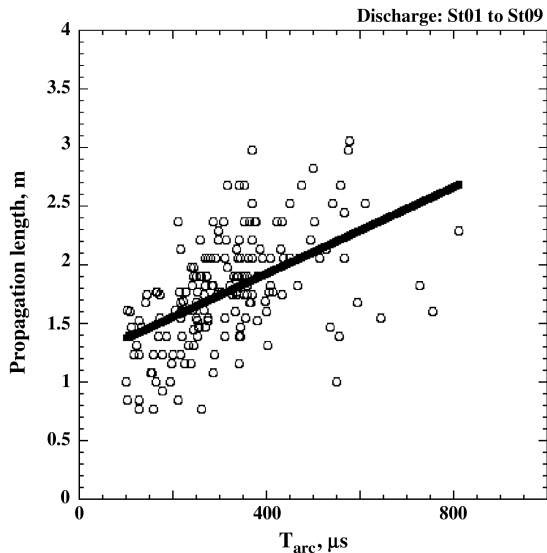


Fig. 16 Relationship between pulse duration T_{arc} and L_p under the LEO environment, $V_b = -800$ V: discharge on St-01 to St-09.

In the LEO environment, L_p also seems to increase with an increase of T_{arc} . When the T_{arc} was less than $100 \mu s$, the minimum L_p was 0.5 m. Contrarily, when the T_{arc} was longer than $500 \mu s$, the minimum L_p was 1 m. The maximum L_p exceeded 3 m in the entire range of T_{arc} . Flashover discharge trends to propagate a longer distance when T_{arc} is long. In addition, our experimental result shows that flashover plasma in the LEO environment propagates a longer distance than that in the GEO environment.

Table 2 summarizes the L_p in the GEO and LEO environments. In the GEO environment, the average L_p is 1.34 m. However, as discussed, when we estimate L_p in the GEO environment, we need to consider T_{arc} realize that the flashover plasma potentially propagates for more distance. In the LEO environment, the ESD tests were carried out at -300 , -500 , and -800 V, and -1 kV. Therefore, the discharge number in the case of $V_b = -1$ kV is lower than that in the case of other bias voltages. In the LEO environment, the average L_p is about 2 m for any bias voltage. The electrons created by a blowoff discharge diverge on the solar array surface because the cover glass potential is positive relative to the cathode spot. Therefore, the differential voltage is also a possible factor in determining L_p . In the LEO environment, the differential voltage is almost the same as the bias voltage [15]. However, Table 2 shows that the bias voltage does not affect L_p in the LEO environment. Although we predicted L_p changes when the differential voltage (i.e., bias voltage) changes, there is no significant difference in L_p . We have not investigated the surface potential before and after discharge in the GEO environment. It is necessary to investigate the effects of differential voltage in the GEO environment because the plasma environment in GEO is different from that in LEO.

In the GEO environment, L_p increases with an increase of T_{arc} . In the LEO environment, we can also see this trend. This invokes the question: is there a limitation of propagation length? To consider this question, we investigated the distribution of T_{arc} in the GEO and LEO environments, which is shown in Figs. 17 and 18. In the GEO

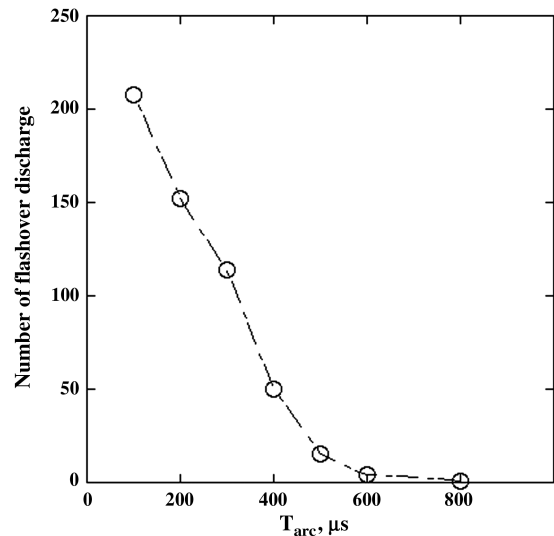


Fig. 17 Distribution of T_{arc} under the GEO environment, $V_b = -6$ kV.

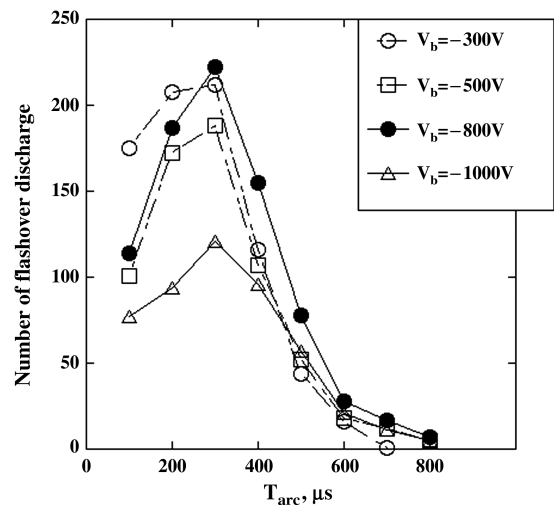


Fig. 18 Distribution of T_{arc} under the LEO environment.

environment, the number of discharges exponentially decreases on T_{arc} . In the LEO environment, although there is a peak around $300 \mu s$ in all bias voltage cases, the number of discharges exponentially decreases as well. A flashover discharge has a cathode spot. The lifetime of a cathode spot of vacuum arc usually decreases exponentially with time [17]. In the GEO environment, the cathode spot of flashover plasma simply follows the theory. In the LEO environment, T_{arc} distribution is different from that of the GEO environment. However, the number of discharges with a T_{arc} of longer than $200 \mu s$ exponentially decreases as observed in the LEO environment. Because the cathode spot cannot be sustained forever, L_p must be limited.

Table 2 Relationship between propagation length and bias voltage

Environment	Bias voltage, V	Propagation length, m				Number of flashover discharges
		Minimum	Maximum	Average	Standard deviation	
LEO	-300	0.39	3.60	2.02	0.52	770
LEO	-500	0.54	3.75	2.12	0.51	653
LEO	-800	0.54	3.75	1.98	0.57	808
LEO	-1000	0.69	3.75	2.00	0.60	482
GEO	-6000	0.38	3.27	1.34	0.50	525

IV. Propagation Velocity

Figure 19 shows the illumination of a flashover discharge on the solar array panel in the GEO environment. We used the IR camera with II to take this picture. We captured the image $20 \mu\text{s}$ after discharge initiation. It is possible for us to investigate the propagation of flashover plasma with this technique. The procedure for analyzing the flashover plasma image is as follows: The IR camera with II captures an image. We apply perspective correction to the original image, and then we obtain the picture shown in Fig. 20. In Fig. 20, the discharge spot is indicated by an arrow. We define the discharge spot as center. The illumination intensity profile on the line in the image is shown at the top with current values $20 \mu\text{s}$ after discharge. In Fig. 20, because neutralized current values are plotted, the point for flashover current does not exist. The neutralized current values decrease with distance from the discharge spot. Because the intensity decreases with distance from the discharge spot, the neutralized current values correlate with the intensity profile. Therefore, visual investigation of the propagation length is possible. In the profile, the discharge spot is indicated by an arrow. The background level of the intensity profile is

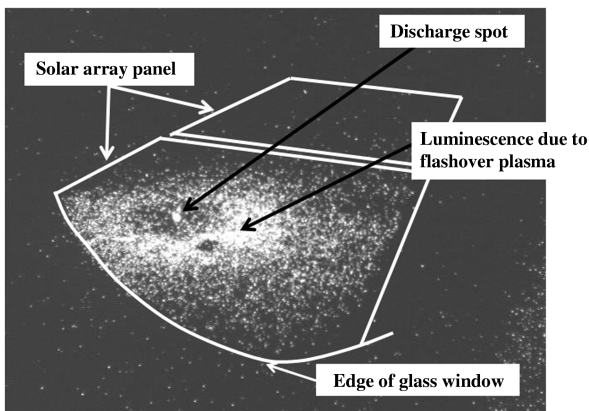


Fig. 19 Luminescence due to flashover plasma $20 \mu\text{s}$ after the discharge.

approximately 30% of the peak. The edge of flashover plasma is defined as the position where the intensity is 40% of that at a discharge spot to avoid the noise portion. To investigate the velocity of flashover plasma propagation, we took images of a discharge when the T_{delay} was 20, 40, 60, 80, 100, 200, and $300 \mu\text{s}$. Figure 21 shows the relationship between the propagation length and the elapsed time (T_{delay}) from discharge inception under the GEO environment. In Fig. 21, the bars express the maximum and minimum of propagation length and the symbols stand for the average values. We calculated the regression curve from the minimum value, average value, and maximum value, as described in Eqs. (5a–5c), respectively:

$$\text{Minimum: } L_p, m = 55 \times T_{\text{delay}}^{0.5}, T_{\text{delay}} \text{ in s} \quad (5a)$$

$$\text{Average: } L_p, m = 106 \times T_{\text{delay}}^{0.5}, T_{\text{delay}} \text{ in s} \quad (5b)$$

$$\text{Maximum: } L_p, m = 185 \times T_{\text{delay}}^{0.5}, T_{\text{delay}} \text{ in s} \quad (5c)$$

We calculated the V_p from Eqs. (5a–5c), separately. Figure 22 shows the relationship between the V_p and T_{delay} from discharge inception under the GEO environment. The curves are described as Eqs. (6a–6c):

$$\text{Minimum: } V_p, \text{ m/s} = \frac{dL_p}{dT_{\text{delay}}} = 22.5 \times T_{\text{delay}}^{-0.5} \quad (6a)$$

$$\text{Average: } V_p, \text{ m/s} = \frac{dL_p}{dT_{\text{delay}}} = 53 \times T_{\text{delay}}^{-0.5} \quad (6b)$$

$$\text{Maximum: } V_p, \text{ m/s} = \frac{dL_p}{dT_{\text{delay}}} = 92.5 \times T_{\text{delay}}^{-0.5} \quad (6c)$$

At $T_{\text{delay}} = 20 \mu\text{s}$, the average V_p is $12 \times 10^4 \text{ m/s}$. Because several authors reported that V_p is in the order of 10^4 m/s [8–11], our result is comparable. After $50 \mu\text{s}$, V_p decelerates to below 10^4 m/s . We

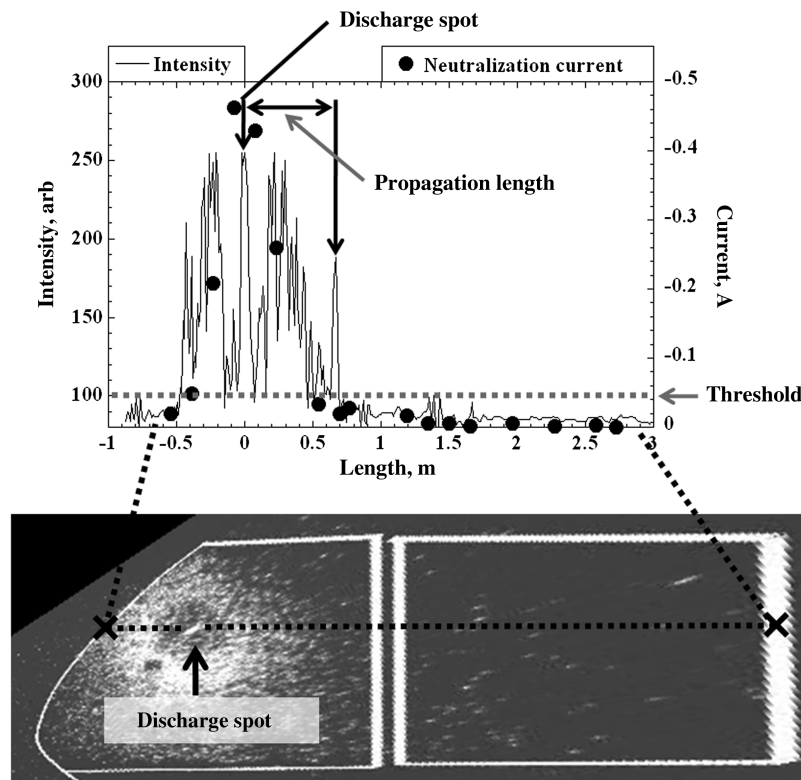


Fig. 20 Flashover image after image processing (bottom) and intensity profile (top).

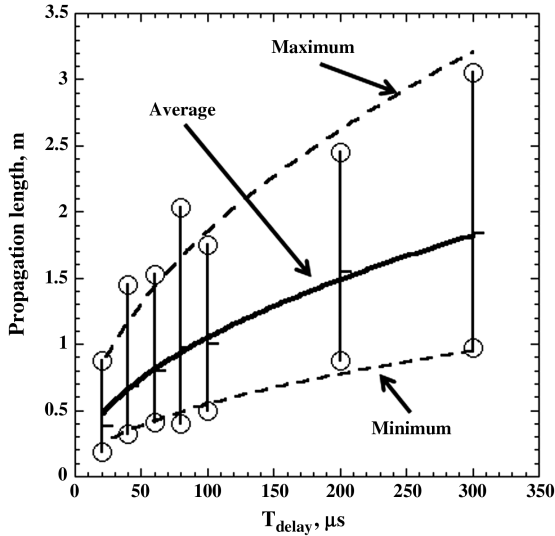


Fig. 21 Relationship between propagation length and elapsed time from discharge inception under the GEO environment.

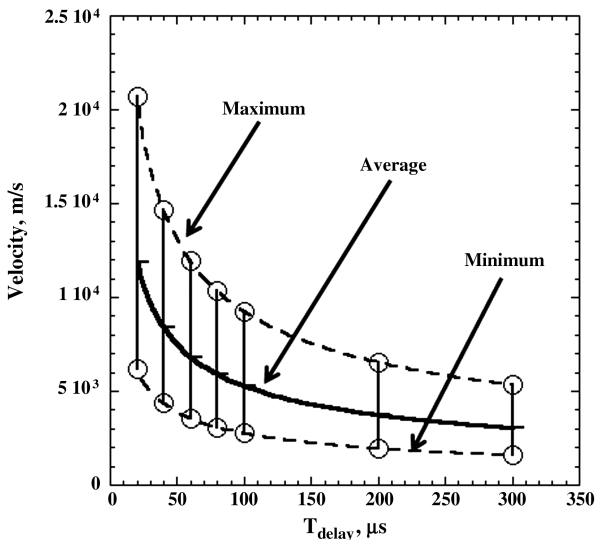


Fig. 22 Relationship between velocity of flashover plasma and elapsed time from discharge inception under the GEO environment.

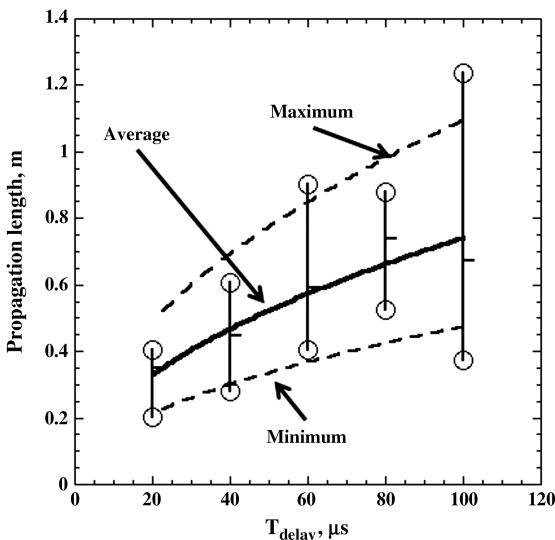


Fig. 23 Relationship between propagation area and elapsed time from arc inception under the LEO environment.

anticipate that flashover plasma does not decelerate enough to be observed when we use small solar array panels.

The V_p under the LEO environment was analyzed in the same way as described in the experiment under the GEO environment. The luminescence of flashover plasma was not observed in the case of $V_b = -300$ or -500 V. We did not capture the image of flashover in the case of $V_b = -1$ kV. Therefore, the dependence of bias voltage on V_p is unknown. Figure 23 shows the relationship between L_p and T_{delay} under the LEO environment. The circles indicate the maximum and minimum L_p . The bar indicates the average values. We calculated the regression curve from the minimum, average, and maximum values, as described in Eqs. (7a–7c):

$$\text{Minimum: } L_p, m = 47 \times T_{\text{delay}}^{0.5}, T_{\text{delay}} \text{ in s} \quad (7a)$$

$$\text{Average: } L_p, m = 74 \times T_{\text{delay}}^{0.5}, T_{\text{delay}} \text{ in s} \quad (7b)$$

$$\text{Maximum: } L_p, m = 110 \times T_{\text{delay}}^{0.5}, T_{\text{delay}} \text{ in s} \quad (7c)$$

The V_p obtained from Eqs. (7a–7c) are described as Eqs. (8a–8c):

$$\text{Minimum: } V_p, \text{ m/s} = \frac{dL_p}{dT_{\text{delay}}} = 23.5 \times T_{\text{delay}}^{-0.5} \quad (8a)$$

$$\text{Average: } V_p, \text{ m/s} = \frac{dL_p}{dT_{\text{delay}}} = 37 \times T_{\text{delay}}^{-0.5} \quad (8b)$$

$$\text{Maximum: } V_p, \text{ m/s} = \frac{dL_p}{dT_{\text{delay}}} = 55 \times T_{\text{delay}}^{-0.5} \quad (8c)$$

Figure 24 shows the relationship between V_p and T_{delay} . At $T_{\text{delay}} = 20 \mu\text{s}$, V_p is 0.8×10^4 m/s in the average, and then it decelerates with time. At $100 \mu\text{s}$, V_p is 4×10^3 m/s on the average V_p curve. As can be seen in Fig. 23, L_p estimated from flashover illumination has significant deviation. Although V_p at $20 \mu\text{s}$ after discharge inception in the LEO environment is slower than that in the GEO environment, we can say that the initial V_p is several tens of km/s, and then the velocity decreases with time. The factor in determining the initial velocity is unknown. As mentioned in the introduction, to estimate the flashover current waveform it is necessary to obtain the L_p and V_p . Because the L_p and V_p in the LEO environment and those in the GEO environment are comparable, we can apply the same model to the current estimation regardless of

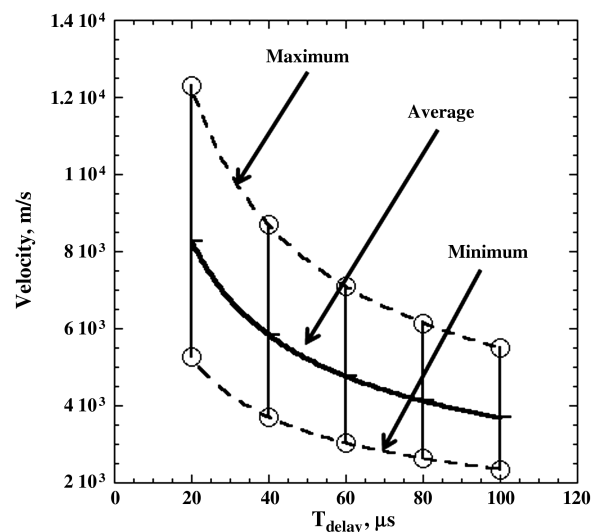


Fig. 24 Relationship between velocity of flashover plasma and elapsed time from arc inception under the LEO environment.

orbital condition. Masui et al. pointed out that the V_p decreases with time on small solar array panels, i.e., 1 m^2 . Therefore, they estimated the flashover current assuming that the flashover plasma decreases with time. The details of their estimation are discussed in [11].

V. Conclusions

We performed an ESD test on 4.8 m [2] solar array panels to investigate the velocity and propagation length of flashover plasma under simulated GEO and LEO environments. To investigate the propagation length of flashover plasma, we measured the neutralized current that flows on each string of the solar array panels using current probes. To investigate the velocity of flashover plasma, we took images of illumination by flashover plasma using an IR camera with II.

The maximum propagation length was 3.4 m under the GEO environment. The average propagation length was 1.76 m. The flashover plasma did not neutralize the entire solar array panel surface within the area inside the diameter of propagation length. The average velocity of flashover plasma was $1.2 \times 10^4 \text{ m/s}$ 20 μs after discharge inception. The average velocity decreased with time, and the velocity was $4 \times 10^3 \text{ m/s}$ at 300 μs after discharge inception.

The maximum propagation length was 3.75 m under the LEO environment. The average propagation length was approximately 2 m. The flashover plasma did not neutralize the entire solar array panel surface within the area inside the diameter of propagation length, which was the same as the result under the GEO environment. This means that we do not need to use a large capacitance to simulate the flashover current in a solar array ESD test in both the GEO and LEO environments. The average velocity was $0.8 \times 10^4 \text{ m/s}$ 20 μs after discharge inception in the LEO environment. As in the GEO environment, the velocity decreased with time. The average velocity was $4 \times 10^3 \text{ m/s}$ 100 μs after discharge inception. As the propagation length was independent from the bias voltage, the differential voltage did not affect the propagation length through the experiment in the LEO environment.

Acknowledgments

This research was supported by the Space Plasma Laboratory, Institute of Space and Astronautical Science, JAXA. We extend our appreciation to Jiro Harada, Yoichi Hagiwara, and Ikuo Yamamoto of Advanced Engineering Services Co., Ltd.

References

- [1] Okumura, T., Ninomiya, S., Masui, H., Toyoda, K., Imaizumi, M., and Cho, M., "Solar Cell Degradation due to ESD for International Standardization of Solar Array ESD Test," *10th Spacecraft Charging Technology Conference on Disk* [CD-ROM], Centre National d'Etudes Spatiales, Toulouse, France, 2007.
- [2] Mateo-Velez, J., Inguibert, V., Roussel, J., Sarraill, D., Levy, L., Boulay, F., Laffont, E., and Payan, D., "ESDs on Solar Cells: Degradation, Modeling, and Importance of the Test Setup," *IEEE Transactions on Plasma Science*, Vol. 36, No. 5, Oct. 2008, pp. 2395–2403. doi:10.1109/TPS.2008.2001835
- [3] Vayner, B., Ferguson, D., and Galofaro, J., "Detrimental Effect of Arcing on Solar Array Surfaces," *10th Spacecraft Charging Technology Conference on Disk* [CD-ROM], 2007.
- [4] Payan, D., Schwander, D., and Catani, J. P., "Risks of Low-Voltage Arcs Sustained by the Photovoltaic Power of a Satellite Solar Array During an Electrostatic Discharge. Solar Arrays Dynamic Simulator, Spacecraft Charging Technology," *Proceedings of the Seventh Spacecraft Charging Technology Conference*, April 2001, pp. 447–453.
- [5] Levy, L., Sarraill, D., Viel, V., Amorim, E., Serrot, G., and Bogus, K., "Secondary Arcs on Solar Arrays: Occurrence, Threshold, Characteristics and Induced Damage," *7th Spacecraft Charging Technology Conference on Disk* [CD-ROM], ESA, Noordwijk, The Netherlands, 2001.
- [6] Katz, I., Snyder, D., and Robertson, E., "ESD Triggered Solar Array Failure Mechanism," Air Force Research Lab. Rept. VS-TR-20001578, 2000, pp. 39–42.
- [7] Toyoda, K., Matsumoto, T., Cho, M., Nozaki, Y., and Takahashi, M., "Power Reduction of Solar Arrays by Arcing Under Simulated Geosynchronous Orbit Environment," *Journal of Spacecraft and Rockets*, Vol. 41, No. 5, 2004, pp. 854–861. doi:10.2514/1.13103
- [8] Okumura, T., Masui, H., Nitta, K., Imaizumi, M., Toyoda, K., and Cho, M., "Environmental Effects on Solar Array Electrostatic Discharge Current Waveforms and Test Results," *Journal of Spacecraft and Rockets*, Vol. 46, No. 3, 2009, pp. 697–705. doi:10.2514/1.41696
- [9] Inguibert, V., Sarraill, D., Mateo-Velez, J., Reulet, R., Levy, L., Boulay, F., and Payan, D., "Electrostatic Discharge and Secondary Arcing on Solar Array: Flashover Effect on Arc Occurrence," *IEEE Transactions on Plasma Science*, Vol. 36, No. 5, Oct. 2008, pp. 2404–2412. doi:10.1109/TPS.2008.2001836
- [10] Kawasaki, T., Hosoda, S., Kim, J., Toyoda, K., and Cho, M., "Charge Neutralization via Arcing on a Large Solar Array in the GEO Plasma Environment," *IEEE Transactions on Plasma Science*, Vol. 34, No. 5, Oct. 2006, pp. 1979–1985. doi:10.1109/TPS.2006.881932
- [11] Masui, H., Toyoda, K., and Cho, M., "Electrostatic Discharge Plasma Propagation Speed on Solar Panel in Simulated Geosynchronous Environment," *IEEE Transactions on Plasma Science*, Vol. 36, No. 5, Oct. 2008, pp. 2387–2394. doi:10.1109/TPS.2008.2003191
- [12] Amorim, E., Payan, D., Reulet, R., and Sarraill, D., "Electrostatic Discharges on a 1 m^2 Solar Array Coupon Influence of the Energy Stored on the Cover Glass on Flashover Current," *9th Spacecraft Charging Technology Conference on Disk* [CD-ROM], JAXA, Tsukuba, Japan, 2005.
- [13] Leung, P., and Bodeau, M., "Plasma Phenomena Associated with Solar Array Discharges and Their Role in Scaling Coupon Test Results to a Full Panel," *8th Spacecraft Charging Technology Conference on Disk* [CD-ROM], NASA, Huntsville, AL, 2003.
- [14] Mashidori, H., Iwasa, M., Nitta, K., and Toyoda, K., "ESD Plasma Propagation Measurements on Large-Scale Solar Panels in Simulated Environment," *26th International Symposium on Space Technology and Science on Disk* [CD-ROM], JSASS, Hamamatsu, Japan, 2008.
- [15] Hastings, D., and Garrett, H., *Spacecraft Environment Interactions*, Cambridge Univ. Press, New York, 1996, pp. 142–198.
- [16] Toyoda, K., Masui, H., Muranaka, T., Cho, M., Urabe, T., Miura, T., Kawakita, S., Gonohe, Y., and Kikuchi, T., "ESD Ground Test of Solar Array Coupons for a Greenhouse Gases Observing Satellite in PEO," *IEEE Transactions on Plasma Science*, Vol. 36, No. 5, Oct. 2008, pp. 2413–2424. doi:10.1109/TPS.2008.2002823
- [17] Lafferty, J. M., *Vacuum Arcs: Theory and Application*, Wiley, New York, 1980, pp. 114–118.

I. Boyd
Associate Editor